Larval dispersal from the Te Tapuwae O Rongokako Marine Reserve: numerical model simulations

Larval dispersal from the Te Tapuwae O Rongokako Marine Reserve: numerical model simulations

Authors

Scott Stephens

Rachel Haskew

Drew Lohrer

John Oldman

Prepared for

The Department of Conservation

Contents

Reviewed by: *Approved for release by:*

Edward Abraham

2 / 09 / 2004   8/

Edward Abraham   Andrew Swales

Formatting checked

Executive Summary

NIWA was commissioned by The Department of Conservation to model larval dispersal from the Te Tapuwae O Rongokako Marine Reserve, with particular focus on predicting the ability of populations within the reserve to populate other habitats along the coast. The five species of interest were bull kelp, kina, limpets, paua and pupu .

This was achieved using numerical models to determine the dispersion "footprint" of larvae released from an inshore point source, based on realistic hydrodynamic forcing. A hydrodynamic model (MIKE21) was calibrated against current-meter measurements made within the reserve. Larval supply was simulated using the MIKE21 Particle Analysis model, for four scenarios: calm weather, average wind and wave conditions, and storm conditions approaching from the south and east.

During calm conditions, larvae tended to settle within about 2 km of the spawning site regardless of species. The mean wind and wave conditions caused a northeast-directed alongshore current that carried larvae towards the northeast. Storm conditions from the south caused the widest dispersal of larvae, also pushing them to the northeast, while storm conditions from the east caused larvae to disperse away from their release point towards the southwest.

Larvae that had longer larval durations dispersed further, because they remained in the water column longer and were subsequently advected further by current flow. Our simulations suggested there will be little export of bull kelp spores from adult populations in the marine reserve to rocky headlands outside the reserve, indicating that local bull kelp populations may be reproductively isolated and localised population declines would not recover quickly via inputs from external sources. Pupu and limpets dispersed northward to Gable End Foreland during average and southerly storm conditions. During the easterly storm they reached as far south as Tatapouri Point, with pupu settling there in higher numbers. Paua dispersed northward to Gable End Foreland during average conditions, and beyond this during southerly storm conditions. During easterly storm conditions, paua dispersed to just south of Tatapouri Point. Kina had the greatest dispersal range of all the species considered in our simulations. This was due to their long larval duration and also their ability to recruit in depths < 30 m below low tide, which opened up a wider settlement area. Kina dispersed further north of Gable End Foreland and south to Tuaheni Point. Plots in Appendix 1 show detailed dispersal patterns.

Whangara Island provided a barrier to northward dispersal from the marine reserve, but larvae were trapped and accumulated on its southern side at a relatively high rate. Therefore the most likely settling point for all larval types spawned in the reserve on the southern side of Te Anaopaikea Point and Whangara Island.

1.   Introduction

NIWA was commissioned by The Department of Conservation to model larval dispersal   from the Te Tapuwae O Rongokako Marine Reserve (Figure 1). In particular, this study aimed to predict the ability of populations within the reserve to populate other habitats along the coast.

This was achieved using numerical models to determine the dispersion "footprint" of larvae released from an inshore point source, based on realistic hydrodynamic forcing. The models were calibrated against current-meter measurements taken within the reserve in September/October 2003, reported by Stephens & Liefting (2003).

The five species of interest were bull kelp, kina, limpets, paua and pupu, found on the rocky reef at the tip of Pariokonohi Point, with some also found on the Hinematikotai Rocks near Te Anaopaikea Point (Figure 1). This report presents estimates of the likely dispersal and settlement range of these species from their spawning sites in the reserve.
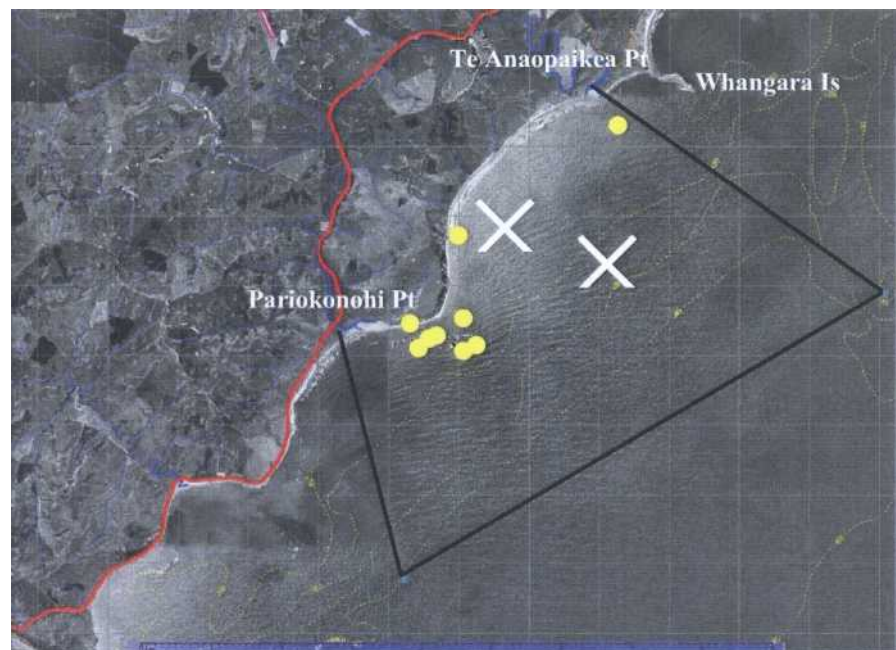

Figure 1.   Aerial photograph of the Te Tapuwae O Rongokako Marine Reserve area. The black lines mark the approximate boundaries of the marine reserve. The 9 yellow dots mark larval release sites, while the 2 white crosses mark the current-meter deployment sites.

2. Modelling methods

Numerical modelling was undertaken using four models. The deepwater wave climate offshore from the marine reserve was extracted from a 20-year WAM hindcast of the New Zealand region (Gorman et al. 2003), and used to calculate mean offshore wave conditions, plus average southerly and easterly storm-wave conditions. These mean waves were then propagated inshore using the wave model SWAN (Young 1999; Booij et al. 1999). Resulting wave radiation stresses were input to a hydrodynamic flow model (MIKE21), which simulated the combined flow effects of tides, winds and waves. A lagrangian particle-analysis model (MIKE21-PA) was then used to simulate larval dispersal in the predicted flow fields.

2.1 Bathymetry grids

All models use a regular square bathymetry grid. The bathymetry grids were created using a combination of data digitised from an existing hydrographic chart (NZ55 and associated fairsheets, supplied by Land Information New Zealand), and detailed data surveyed by ASR Ltd and supplied by the Department of Conservation. All positions were rotated 45° anticlockwise about NZMG origin X = 2946630 Y = 6261270 before gridding, to align the coast with vertical in the models. The 45° rotation was suggested both by the alignment of the coast and the measured currents at the offshore site.

Three grids were created, a broad-scale grid with 270 m-square cells with nested grids using 90 m-square and 30 m-square cells (Figure 2). To calibrate the model it was necessary to use a flux boundary based on the current measurements, which required equivalent fluxes through both the north and south boundaries. Therefore the northern boundary of the 270 m grid was set equal to the southern boundary, and the bathymetry smoothed back to meet Gable End Foreland (Section 3). Details of the grid limits and data rotation points are given in Table 1. Vertical grid datum is lowest astronomical tide, which corresponds to the datum of navy chart NZ55. Water level in the simulations was set to the approximate mean sea level of 1.225 m above datum. Low tide is taken as being 0.8 m below mean sea level, or 0.425 m above model datum.
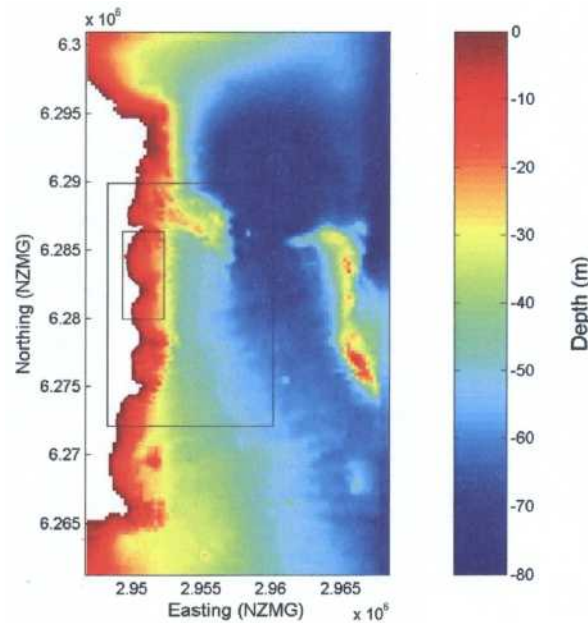
Figure 2.   Shaded colour map of the bathymetry grids. The black boxes mark the outlines of the nested 90 m (area 2) and 30 m (area 3) grids inside the 270 m (area 1) grid. Depth data were rotated 45° anticlockwise about NZMG origin X = 2946630 Y = 6261270 before gridding, to align the coast with vertical in the models.

Table 1:   Cell-size and limits (New Zealand Map Grid coordinates) of the three regular grids used for numerical modelling. Table data have been rotated 45° anticlockwise about NZMG origin X = 2946630 Y = 6261270.

Cell size (m)	X lower-left	Y lower-left	X top-right	Y top-right
270	2946630	6261270	2968500	6300960
90	2948250	6272070	2960130	6289890
30	2949330	6279900	2952300	6286380

2.2   Wave climate predictions

Historically, wave data coverage of New Zealand's coast has been poor, particularly for directional records.   With very few data sets available of more than one year's duration, it has been difficult to establish accurate wave climatologies. To help fill in the gaps in our wave records, the WAM wave generation model has been implemented over a domain covering the Southwest Pacific and Southern Oceans. The model has been used to hindcast the generation and propagation of deep-water waves incident on the New Zealand coast over a 20-year period (1979-98), using winds from the

European Centre for Medium Range Weather Forecasting (ECMWF). The resulting synthetic climatology is expected to provide a valuable tool for researchers and coastal planners (Gorman et al. 2003).

For this study, the 20-year hindcast was extracted for 178.295°E, -38.670°S, a deepwater site corresponding with the outer edge of the large-scale 270 m grid (Section 2.1). Of the 61360 3-hourly wave statistics, the mean significant wave height H_s (average of the highest $1/3^{rd}$ of waves), mean wave approach direction D (coming from) and mean wave period T_m were 1.7 m, 205° and 7.0 s respectively. About 70% of all waves approach from ESE through S (Table 2). We define southerly storm waves as those storm waves approaching from south of east, and these make up 74% of storm waves, or 2.6% of all waves. We define easterly storms as those storm waves approaching from east or north of east, and these make up 26% of storm waves, or 0.9% of all waves. Waves of 1 m or less in height occurred 16% of the time (e.g. Figure 3). Figure 3 can be used to estimate the frequency of occurrence of deepwater waves near the marine reserve, and Figure 4 shows their relative height and direction distribution.
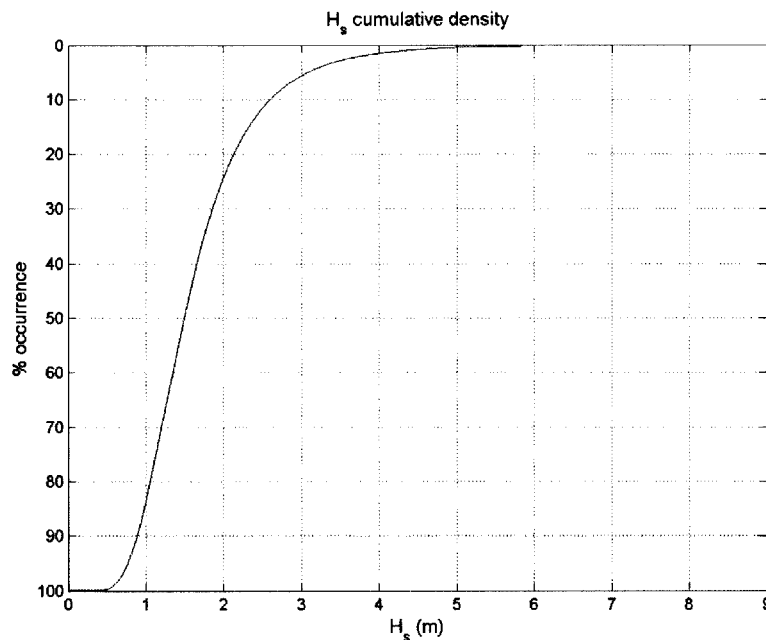

Figure 3.   Cumulative density curve of significant wave height H_s from the 20-year wave hindcast offshore from the marine reserve.

Wave Rose for Te Tapuwae WAM

n = 61,360
Frequency
Interval = 5%
Calm = 0%

Wave Height (m)

>0 - 0.5
0.5 - 1
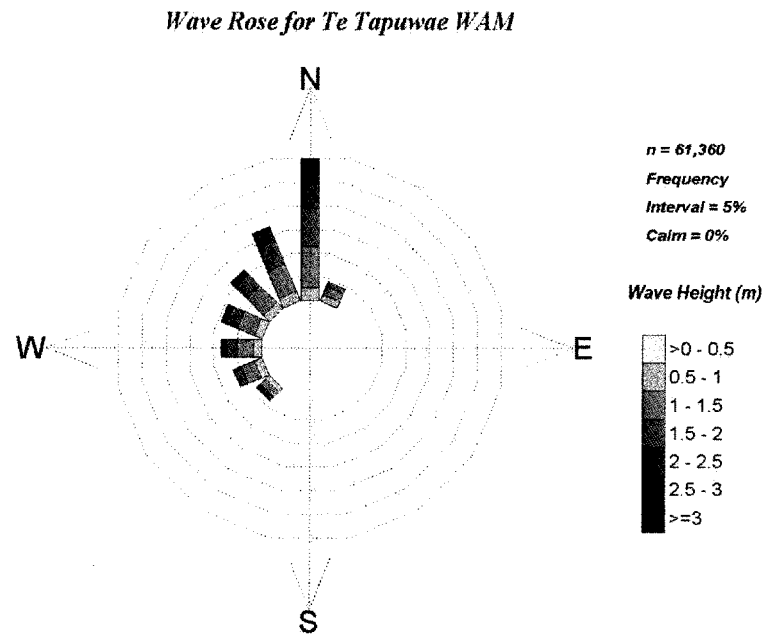1 - 1.5
1.5 - 2
2 - 2.5
2.5 - 3
>=3

Figure 4.   Wave rose of significant wave height and mean wave direction from the 20-year wave hindcast offshore from the marine reserve. Directions are shown as to where the waves are moving.

Table 2.   Percent approach direction (coming from) of waves predicted by the 20-year WAM hindcast. Storm waves were selected using a peaks-over-threshold method with a 2-day threshold. Percentages are given to the nearest percent and only directions with occurrence greater than 0% are shown.

Approach Direction	S	SSW	SW	NNE	NE	ENE	E	ESE	SE	SSE
All (n = 61360)	30	5	1	1	5	8	9	10	13	18
Storm (n = 2132)	37	5	0	2	8	8	8	8	9	15

2.3   Wave-model: SWAN

SWAN is a numerical wave model developed to obtain realistic estimates of wave parameters in coastal areas, lakes and estuaries from given wind-, bottom-, and current conditions. The model is based on the wave action balance equation (or energy balance in the absence of currents) with sources and sinks. SWAN (acronym for Simulating WAves Nearshore) is a third-generation wave model with first-, second-

and third-generation options. Good introductions into the background of SWAN are (Young 1999) and (Booij et al. 1999).

The SWAN model was forced by applying wave conditions extracted from the WAM hindeast to all open boundaries of the 270 m grid (e.g. Figure 5). SWAN was run using default physical parameters, that included third-generation mode physics, wave breaking, bottom friction, and quadruplet and triad wave-wave interactions in deep and shallow water respectively.

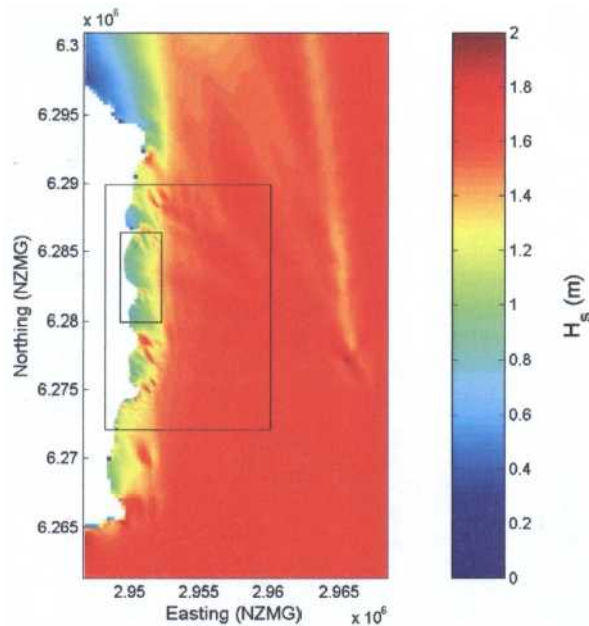Wave radiation stresses were output for all three grids

Figure 5.   Simulated wave height from SWAN using the mean wave statistics ($H_s = 1.7\text{m}, D = 205'$, $T_m = 7.0$ s) at the open boundaries (statistics from the 20-year WAM hindeast).

2.4   MIKE21 hydrodynamic flow model

The MIKE 21 hydrodynamic flow model is a modeling system for 2-dimensional free-surface flows. MIKE 21 is applicable to the simulation of hydraulic and environmental phenomena in lakes, estuaries, bays, coastal areas and seas. It may be applied wherever stratification can be neglected. Temperature measurements indicated that the water column was unstratified during the ADCP deployment (Stephens & Liefting

2003), but the main reason for choosing the 2-dimensional MIKE21 model ahead of a 3-dimensional model was its ability to include forcing by wave radiation stresses.

Waves are a dominant forcing mechanism in shallow water near the coast, and were primarily responsible for the poor calibration obtained at the inshore current-meter site (Section 3). These littoral currents are very effective in ejecting larvae spawned in shallow inshore waters out into the broad-scale tidal and wind-induced flows. Appendix 2 illustrates that the dispersal modelling would be much poorer without the wave-induced currents. Although we cannot reproduce the high variability of these littoral currents because we are applying monochromatic wave conditions, we can include a steady littoral current of the right order of magnitude. The inclusion of wave radiation stresses is limited to a stationary forcing field for the duration of the simulation, such as the mean wave radiation stresses over the deployment period.

The hydrodynamic model included forcing by tides, wind and wave radiation stresses. Radiation stresses were only input for the inner 30 m nested grid.

2.5   MIKE21 particle-analysis model

The particle-analysis model is based on the random walk technique where an ensemble of "particles" (larvae) is tracked (i.e. lagrangian technique). The "particles" move due to the advective current and turbulent fluctuations. The advective velocities are obtained from the hydrodynamic (HD) simulations, whereas the turbulent contributions are controlled by dispersion coefficients.

Larval releases were represented by the instantaneous release of 1000 "particles" at each source point, the 1000 "particles" having a combined concentration of 1 kg m^{-3}. The concentration is somewhat arbitrary, but can be converted to a meaningful number by stating its equivalence to the fecundity of the organism, e.g. 1 kg m^{-3} = fecundity, where fecundity is the number of larvae or eggs released in a single spawning episode. In this way the dilution of larvae numbers through dispersal is easily converted from particle concentration by the relationship

$$1 larva = \frac{1}{fecundity} kg m^{-3}$$ eqn 1

and rounding to the nearest integer. Each "particle" therefore consists of many individual larvae.

The larvae "particles" were represented using a 1st-order sedimentation process. In this scheme each "particle" was treated as a mass of sediment, the sediment was regarded as fully mixed over the depth, and the settling of sediment took place with a constant settling velocity, thereby reducing the remaining mass of each particle in suspension. Thus the settling of particle sediment mass represents the settling of larvae on converting the sediment concentration back to larvae numbers. The "particles" were advected with the local velocity profile, which was specified as logarithmic in the vertical.

The flow fields calculated in MIKE21 and used for advection of particles in the particle-analysis model are calculated in a grid of a certain extent in time and space. Physical flow processes, however, occur at different spatial and temporal scales with a continuous spectrum ranging from tiny molecular agitation to large-scale oceanic currents. It is simply too computationally expensive to calculate the tiny molecular processes across the spatial scales of the large domain, which means the model is simplified into grid cells much larger than the intermolecular spacing associated with molecular agitation processes. To take these effects into account, a dispersion coefficient is applied, which is a mathematical artifact arising from the spatial averaging rather than an actual physical process. This allows more realistic larvae dispersal. Selecting dispersion coefficients is difficult, and ideally these coefficients are obtained from a calibration process where simulated and measured concentration fields are compared (DHI Water and Environment 2003). In practise these calibration data are seldom available, as was the case for the present study. Dispersion coefficients in both the horizontal and vertical directions were proportional to the predicted currents. In the horizontal, the minimum dispersion coefficient was set to 0.01 $m^2 s^{-1}$ and the maximum value of 1 $m^2 s^{-1}$. In the vertical the limits for the dispersion coefficient were 0 and 0.01 $m^2 s^{-1}$. These values are at the lower end of recommended dispersion coefficients (e.g. longitudinal 0.27-6.75 $m^2 s^{-1}$) for the grid size and timestep used (DHI Water and Environment 2003), and also correspond to values used in other model studies within New Zealand (Oldman & Black 1997, Green et al. 1999, Green & Oldman 1999, Oldman & Swales 1999, and Oldman and Senior 2000). Further details of the particle-analysis simulations specific to the individual larval types are presented in Section 4.2.

3. Model calibration

To get currents flowing correctly in the interior of the model domain, it is first necessary to accurately specify the hydrodynamics (e.g. water levels, fluxes) at the model's open boundaries. Specifying the boundary conditions for an open-coast model provides a difficult challenge, particularly where tidal component is small relative to other forcings that aren't easily measured or predicted. Some of the flow events (changes in speed and direction) generated by larger, ocean-scale forcing (e.g., by the East Auckland Current, the Wairarapa Coastal Current and density-driven eddies) are very difficult to quantify without a very detailed analysis of satellite images and offshore measurements. These processes could not be represented in the forcing applied to the model's open-sea boundaries.

Often, tidal water level variations are applied to the open model boundaries, and where these are relatively large they provide a good forcing of the model. A complicating factor is the presence of amphidromes off the North Island east coast in several of the major diurnal (occur once per day e.g. K_1, P_1, O_1, Q_1) and semi-diurnal (occur twice per day e.g. S_2, K_2) tidal constituents (Walters et al. 2001). At an amphidrome, the sea level amplitude of the tidal constituent is zero, but the tidal velocity reaches a maximum. The presence of the amphidromes meant that the extraction of water levels from an existing New Zealand tidal model (Walters et al. 2001) provided a poor forcing for our model.

Fortunately, current measurements from the current-meter deployment could be extrapolated to form suitable open boundary forcing conditions. This was done as follows:

1. The current measured at the offshore current-meter site was split into cross-shore and alongshore components coinciding with the model grid alignment.

2. The flux through the southern boundary required to reproduce the alongshore current velocity was calculated.

3. The southern and northern boundaries were set equal to the calculated flux. To conserve mass in the simulation, the bathymetry at the northern boundary was set to equal the southern boundary (270 m grid only, Figure 2). This bathymetry alteration was far outside the main region of interest and was considered to have negligible impact on the larvae dispersal results.

4. The offshore (eastern) boundary was set to zero-flux to restrict flow to the alongshore direction. This was required to force the model using the flux boundaries, and was justified by the fact that most of the flow was alongshore at the offshore current-meter site.

5. A 30-minute time lag was applied between the forcing boundaries to allow for the expected shallow-water phase lag.

Figure 6 shows the resulting calibration. The calibration plot shows the simulated currents at the offshore current-meter site, compared with the measured currents at this site, depth-averaged between 5.5 and 17.5 m. Cross-shore currents are not well reproduced by the model, but this is expected since the model was only forced in the alongshore direction. In the alongshore direction the model does well, it reproduces the timing of flow reversals and the flow magnitudes are close. Furthermore the cumulative flow past the current-meter site has the right order of magnitude and exhibits similar trends (Figure 7). We are therefore confident that this method of forcing the model is adequate for reproducing the main flow events with the right order of magnitude.
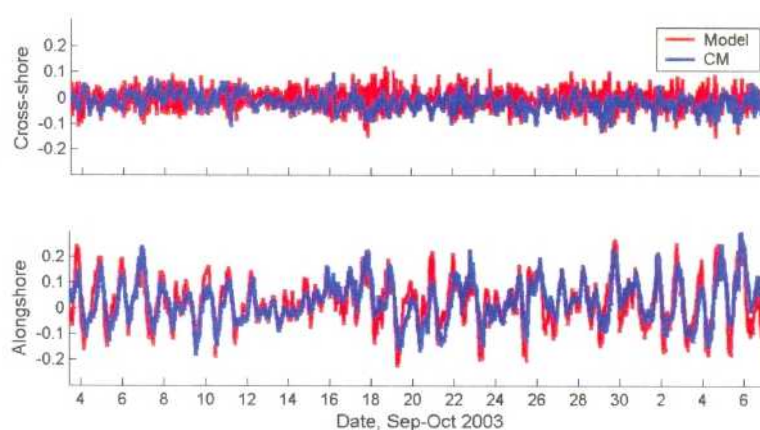

Figure 6. Calibrated cross-shore and alongshore currents using an open boundary flux based on the alongshore current measured at the offshore current-meter site.

It is desirable to be able to model time periods other than those for which the current-meter was deployed, when there are no flow data to apply at the open boundaries. A tidal harmonic analysis was undertaken on the alongshore and cross-shore components of the measured currents at the offshore site, the results of which can be used to reconstruct a tidal current timeseries for any time period. In this way a tidal flux boundary was created using the method described on the preceding page. The model

was then forced with the tidal flux boundary, wind measured at Gisborne Airport, and the wave radiation stress created by the average wave conditions measured during the deployment (H_s = 1.0 m, D = 90°, T_m = 7.2 s). Figure 8 shows the resulting calibration.
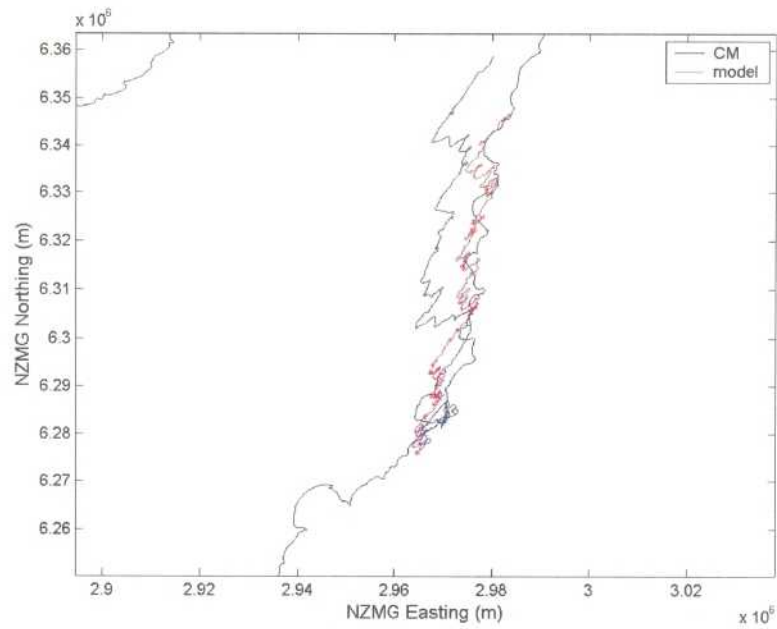

Figure 7.   Cumulative vector plot of measured and calibrated model currents, using an open boundary flux based on the alongshore current measured at the offshore current-meter site.
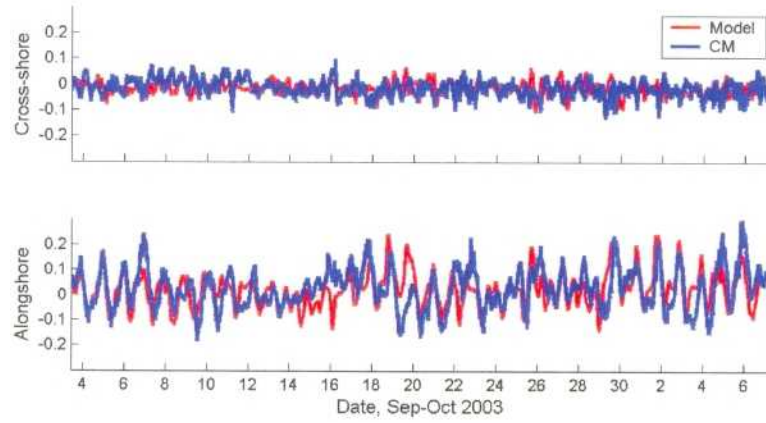
Figure 8.   Calibrated cross-shore and alongshore currents using an open boundary flux based on the tidal component of the measured alongshore current, wind measured at Gisborne Airport and mean wave conditions during the deployment.